Geophysical Journal International

The Mw 6.3, 2009 L'Aquila earthquake: source, path and site effects from spectral analysis of strong motion data

Journal:	*Geophysical Journal International*
Manuscript ID:	GJI-09-0397
Manuscript Type:	Fast Track Paper
Date Submitted by the Author:	29-Jul-2009
Complete List of Authors:	Bindi, Dino; INGV, Sezione Milano-Pavia Pacor, Francesca; INGV, Sezione Milano-Pavia Luzi, Lucia; INGV, Sezione Milano-Pavia Massa, Marco; INGV, Sezione Milano-Pavia Ameri, Gabriele; INGV, Sezione Milano-Pavia
Keywords:	Earthquake ground motions < SEISMOLOGY, Earthquake source observations < SEISMOLOGY, Site effects < SEISMOLOGY, Seismic attenuation < SEISMOLOGY, Fourier analysis < GEOPHYSICAL METHODS

The Mw 6.3, 2009 L'Aquila earthquake: source, path and site effects from spectral analysis of strong motion data

D. Bindi[1], F. Pacor[1], L. Luzi[1], M. Massa[1] and G. Ameri [1]

[1]Istituto Nazionale di Geofisica e Vulcanologia, Via Bassini 15, 20133 Milano, Italy

Summary

The strong motion data of April 6, 2009 L'Aquila (Central Italy) earthquake (Mw=6.3) and of 12 aftershocks (4.1≤Mw≤5.6) recorded by 56 stations of the Italian strong motion network are spectrally analyzed to estimate the source parameters, the seismic attenuation, and the site amplification effects. The obtained source spectra for S-wave have stress drop values ranging from 2.4 to 16.8 MPa, being the stress drop of the main shock equal to 9.2MPa. The spectral curves describing the attenuation with distance show the presence of shoulders and bumps, mainly around 50 and 150km, as consequence of significant reflected and refracted arrivals from crustal interfaces. The attenuation in the first 50 km is well described by a quality factor equal to $Q(f) = 48 f^{0.6}$ and a geometrical spreading exponent equal to 0.75. Finally, the horizontal-to-vertical spectral ratio provides unreliable estimates of local site effects for those stations showing large amplifications over the vertical component of motion.

Introduction

On April 6th, 2009 at 01:32:39 GMT a magnitude Mw=6.3 [Global Centroid Moment Tensor Project, www.globalcmt.org] earthquake struck the Abruzzo region (Central Italy). The epicentral area corresponds to the upper and middle Aterno valley which is characterised by a complex tectonic evolution reflected by the high variability of the geologic and geomorphologic patterns. The valley is superimposed on a Quaternary lacustrine basin of tectonic origin. The depth of the Quaternary deposits is variable, from about 60m in the upper Aterno valley to more than 200m in the middle Aterno valley (Bosi & Bertini, 1970). The L'Aquila town, located at about 6 km northeast to the mainshock epicenter, as well as several villages located nearby, suffered heavy damages and the casualties were nearly 300. Accordingly to the normative for the Italian territory, the area struck by the L'Aquila earthquake is classified as a zone characterized by high level of seismic hazard (*Gruppo di Lavoro MPS,* 2004). In terms of probabilistic hazard assessment, the maximum peak ground acceleration having the probability of 10% of being exceeded in 50 years is 2.55 m/s^2.

The mainshock was followed, within the first week, by seven aftershocks with moment magnitude greater than or equal to 5, the two strongest ones occurred on April 7th (M_w=5.6) and April 9th (M_w=5.4). The rapid dissemination through the online ITACA database (http://itaca.mi.ingv.it) of the strong motion recordings relevant to the 13 strongest earthquakes of the sequence, allows us to investigate the contribution of different terms to the observed ground shaking. In this study, the acceleration spectra are jointly analyzed to estimate the source parameters, the seismic attenuation, and the local site amplification effects.

Strong-motion data set

For this work, we analyzed 264 recordings from 56 strong-motion stations triggered by the April 6, 2009, L'Aquila earthquake and 12 aftershocks (Ameri *et al*., 2009). These stations belong to the Italian Strong Motion Network (RAN), managed by the Italian Department of Civil Protection (DPC). They are equipped with three-component sensors set to 1 or 2 g full-scale, coupled with 24-bit digitizers with a sampling rate of 200 samples per second. Data from 13 earthquakes (Table 1) with $4.1 \leq Mw \leq 6.3$ and recorded at distances smaller than 200 km are downloaded from the ITACA database (Luzi *et al*., 2008). Figure 1 shows the location of the epicenters and recording stations, as well as the mainshock recorded by a station (AQK) installed in the town of L'Aquila.

The recorded waveforms are processed following the standard ITACA procedure (Massa *et al*., 2009), The Fourier spectra have been calculated for windows starting about 1 s before the S-wave onset and ending when 90% of the total energy after the S-wave onset has been released. The minimum and maximum durations were constrained to 5 and 30 s respectively. Recordings at distances smaller than 10 km have been visually inspected, selecting a window encompassing the whole strong motion phase. The acceleration Fourier spectra were smoothed using the Konno & Ohmachi (1998) algorithm, fixing the smoothing parameter b to 40. The spectral amplitudes are analyzed in the frequency range from 0.3 to 25 Hz.

Method

We apply a two-step non-parametric approach (GIT) (e.g. Castro *et al*., 1990) to describe the observed spectral amplitudes $D(f,r)$ in terms of source $S(f)$, attenuation $A(f,r)$ and site $Z(f)$ contributions:

$$\log_{10} D(f, r_{ij}) = \log_{10} A(f, r_{ij}) + \log_{10} \tilde{S}_j(f) \qquad (1)$$

$$\log_{10} R(f, r_{ij}) = \log_{10} Z_i(f) + \log_{10} S_j(f) \qquad (2)$$

where r is the hypocentral distance, f the frequency, i=1…N_{sta} spans the set of available stations, j=1…N_{eve} spans the set of considered earthquakes $\tilde{S}_j(f)$ is a scalar which depends on the size of the j-th source and $R(f,r_{ij})$ represents the observed spectral values corrected for attenuation $A(f,r_{ij})$. Considering the whole set of available recordings, equations (1) and (2) define two linear systems that we solved in a least-squares sense. In the first step, the attenuation-with-distance curves $A(f,r)$ are obtained by solving the linear system (1) in a least-square sense. The inversion is performed for each frequency and the distance range is discretized into M bins Δr km wide.In the second step, the residuals $R(f,r_{ij})$ are used to determine the source spectra $S_i(f)$ and the site amplification functions $Z_j(f)$ by solving system (2) in a least-square sense, without assuming any a-priori functional form to describe the source spectra. A standard source model (Brune, 1970) is later fit to the non-parametric solutions to determine the source parameters. To fix one unresolved degree of freedom affecting solutions of system (1), the attenuation curves $A(f,r)$ are constrained to 1 at a reference distance r=r_{ref}, irrespective of frequency. Moreover, the $A(f,r)$ curves are constrained to be smooth functions of distance (Castro *et al*., 1990). In the second step, the trade-off between the spectral source amplitude and site

amplifications is resolved by assuming a reference site Z_{ref} whose site amplification factors are constrained to values a-priori selected.

Spectral attenuation with distance

The first step of the inversion allows us to determine the spectral attenuation curves *A(f,r)* as function of distance. The distance range from 6 to 201 km is divided into 40 bins 5 km wide. The *A(f,r)* is constrained to 1 at r_{ref} =11km, irrespective of frequency. Figure 2 (top panel) shows the *A(f,r)* curves obtained by vectorially summing the two horizontal components (i.e., $\sqrt{NS^2 + EW^2}$). The unit covariance matrix computed for the first step (see Figure CM2 in the complementary materials) shows that the source-to-station geometry well constrains the attenuation for the selected spatial resolution, especially for distances up to 70 km. The quite narrow spread observed around the diagonal elements means that the error propagation among unknowns is restricted to attenuation values for close distance bins. Finally, the covariance matrix confirms that the trade-off between the attenuation and source blocks is reduced.

The rate of attenuation with distance varies over the analyzed distance range. In particular, the curves decay fast in the first 50 km, then they flat or slope upward depending on the frequency value. For distances larger than about 70 km the curves generally decay with distance less rapidly than in the first 50 km, but the frequency dependence increases. Finally, for distances from 100 to 150 km and frequency smaller than 2Hz, the spectral attenuation curves have small bumps. The features showed by *A(f,r)* are in agreement with several observations made worldwide. Previous studies demonstrate that the boundary between the fall-off of the direct waves and the emergency of lower crustal or Moho reflections can lead to fairly constant amplitudes on distance ranges that depend on several factors, such focal depth, crustal thickness, crustal-velocity gradient, among others (e.g. Burger *et al.*, 1987; Sommerville & Yoshimura, 1990;

Atkinson & Mereu, 1992; Mori & Helmberger, 1996). The behavior of the spectral attenuation curves shown in Figure 2 (top panel) suggests that reflections and refractions from crustal interfaces are significant in the investigated area for distances between 50 and 70 km and around 150 km, in agreement with previous results obtained in central Apennines (Ponziani *et al*., 1995; *Bindi et al*., 2004). Since an estimate of the quality factor Q for S-waves is important for many seismological investigations, we repeat the inversion (1) but selecting only recordings at distances in the range 5-50 km, where a monotonic attenuation with distance occurs (Figure 2). In order to improve the spatial resolution, we set Δr = 2.5 km, and the spectral attenuation is constrained to 1 at r_{ref} =8.5 km. The covariance matrix for the selected settings is shown in Figure CM3 of the complementary materials.

The attenuation curves are described in terms of geometrical and anelastic attenuation, considering the following model:

$$A(f,r) = \left(\frac{8.5}{r}\right)^{n} \exp\left(\frac{-\pi f (r-8.5)}{\beta Q}\right) \qquad (3)$$

where n is the geometrical spreading coefficient, β = 3.2 km/s is the selected mean shear wave velocity, and Q is the frequency-dependent quality factor. The parameters n and $Q(f)$ are determined in a least-squares sense by fitting model (3) to the set of spectral attenuation curves obtained solving system (1). The obtained solution corresponds to n=0.75 and to Q(f) values shown in Figure 2 (bottom). By fitting a power function to Q(f), the best least-squares solution is $Q(f) = 48 f^{0.6}$.

Site amplifications and sources

In the second step, the observed spectral amplitudes, corrected for attenuation, are inverted to separate the source contribution from the site amplification effects System (2) is solved constraining to zero the logarithm sum of the site amplification functions *Z(f)* of two rock sites, namely Celano (CLN) and Leonessa (LSS), whose locations are shown inFigure 1. The inversion is performed considering each component of motion separately.

Site effects

The unit covariance matrix relevant to the second step (see Figure CM4 in the complementary material) confirms that the trade-off between source and site is well resolved and the propagation of error among different unknowns is negligible. The diagonal elements show that the amplification factor for the error propagation from data to solution is generally smaller than 0.5 except for site terms relevant to stations that recorded only one earthquake. In the following, we discuss the results only for stations with at least 3 records and located within 60 km from the mainshock epicenter. In Figure 3, the GIT site amplifications obtained for the NS and vertical component of some stations are compared to the north-south (NS) horizontal to vertical (H/V) spectral ratio (Lermo & Chavez-Garcia, 1993). The comparisons for the other stations and for the east-west (EW) component are shown in the complementary materials. In Figure 3, stations AQG and AQV are two out of 6 stations composing a strong-motion array installed by DPC in 2001 across the upper Aterno Valley to detect the variation of the ground motion for different geological conditions. These stations are located within the surface projection of the L'Aquila mainshock fault and are at distances less than 5 km from the mainshock epicenter. Station AQG is installed on outcropping bedrock but both the GIT

and the H/V show amplifications over the range 1-6 Hz, probably due to rock fracturing and/or weathering, as observed in the field. Although the two techniques provide a similar trend for the site amplifications, some differences are observed in the results, such as the peak at 0.6 Hz, which is detected only in the H/V ratio. Station AQK is installed close to L'Aquila downtown. The GIT results for the NS component detects the fundamental frequency of resonance at 0.6 Hz, but significant amplifications are also observed over the range 1 – 2 Hz, whereas the vertical component is strongly amplified between 1 and 3Hz. The H/V curve well depicts the amplification at 0.6 Hz but misses the pattern of amplification between 1 and 3 Hz. For station AQV, the GIT and H/V peaks at about 2.5 Hz are in good agreement with the fundamental frequency of resonance estimated from the available shear wave velocity profile (http://itaca.mi.ingv.it).

Station Antrodoco (ANT) is installed over slope debris. The GIT results show significant amplification only for the horizontal component, in good agreement with the H/V. For sites located on deep alluvial deposits, as Avezzano (AVZ) and Norcia (NOR), the GIT results show remarkable amplifications for both the horizontal and vertical components, causing significant differences with respect to the H/V. Station Celano (CLN) is installed on a rock site and it has been selected as one of the two reference sites in the GIT inversion. It shows an almost flat H/V curve, with the presence of a small peak between 1 and 2 Hz. The large uncertainty affecting the amplitude of this peak (see Auxiliary materials), as well as the absence of any peak in the H/V computed considering ambient noise measurements (http://esse4.mi.ingv.it), suggest that its origin might not be related to local site effects.

Both the GIT and H/V results for Bazzano (BZZ) do not identify any amplification peak. This result deserve further investigations since Onna, a settlement distant less than 2 km from BZZ and located on a similar geological setting, suffered very heavy damage by the mainshock. Differently from BZZ, the H/V at Onna, computed considering the strong-motion data recorded by a temporary station (http://rais.mi.ingv.it/statiche/ABRUZZO-2009/main.html), shows a peak of amplification at about 2.5 Hz (Marzorati, personal communication, 2009), consistent with the shear wave velocity profile estimated from array noise measurements (Picozzi and Parolai, personal communication, 2009). Although the role of the building vulnerability should be taken into account, the differences in the local site conditions seem to have played an important role in determining the observed damage pattern.

Source functions

The source functions obtained for each component are composed into a single source spectrum for each earthquake (i.e. $\sqrt{NS^2 + EW^2 + Z^2}$) to determine the S-wave source parameters. The source parameters are computed describing the obtained spectra in terms of a standard model (Brune, 1970). To avoid biases in the estimation of the source parameters due to the limitation in low frequency range (f >0.3 Hz), the seismic moments of the four strongest earthquakes (Mw ≥5.3) are constrained to the values provided by Harvard-CMT (Table 1). The results are shown in Figure 4 and the obtained source parameters are listed in Table 1. The seismic moment M_0 and the corner frequency fc are used to determine the stress drop $\Delta\sigma$ and the source radius R_0 using standard relationships (Keilis-Borok, 1959; Brune, 1970).

$$R_0 = \frac{2.34\beta}{2\pi f_c} \qquad (4)$$

$$\Delta\sigma = \frac{7M_0}{16R_0^3} \qquad (5)$$

The differences between the Mw of RCMT-INGV [http://www.bo.ingv.it/RCMT/]catalog and the one computed by applying the Hanks & Kanamori (1979) relation to the seismic moments estimated in this study, do not exceed 0.3 magnitude units (Table 1), suggesting that the limitation in the bandwidth did not seriously biased the estimates of the seismic moment. The estimated corner frequency for the main shock is 0.24 Hz, corresponding to a Brune radius of 5.46 km and a stress drop of 9.2 MPa. The stress drop of the 13 considered earthquakes varies between 2.4 to 16.8 MPa. Table 1 also lists the root-mean-square stress drop ($\Delta\sigma_{RMS}$) computed following Hanks & McGuire (1981). The general agreement between the Brune stress drop and $\Delta\sigma_{RMS}$ confirms the reliability of the high frequency level of the acceleration source spectra estimated considering the Brune model. Finally, the results on the source parameters are summarized in Figure 4 (bottom panel), . The distribution of seismic moment versus source dimension parameters is well approximated by a constant stress drop scaling, considering the average stress drop of 9.4 MPa.

Conclusions

The strong motion recordings of 13 earthquakes of the April 2009 L'Aquila sequence have been spectrally analyzed to determine the source parameters, the spectral attenuation and the site amplification functions. The stress drop of the main shock (Mw=6.3) and of the three largest aftershocks (5.3≤Mw≤5.6), computed constraining the seismic moment to the values provided by Harvard-CMT, varies between 9.2 and 16.8 MPa. The average stress drop for the 13 earthquakes is 9.4 MPa, in good agreement with the average $\Delta\sigma_{RMS}$ (11.4MPa). These values are larger than the average stress drop of 1.9 MPa estimated by applying the same technique to the 1997-98 Umbria-Marche sequence (Bindi *et al.*, 2004), but within the variability observed in Central and Southern Apennines (e.g. Rovelli *et al.*, 1988]) The attenuation with distance curves show shoulders and bumps, mainly around 50 and 150 km, suggesting the presence of significant reflected and refracted arrivals from crustal interfaces and Moho. The shear-wave quality factor Q for distances smaller than 50 km is well described by $Q(f) = 48 f^{0.6}$, with a geometrical spreading exponent *n* equal to 0.75.

The site amplifications are significant for several stations. In particular, the amplification over the vertical component observed for several stations, limits the applicability of horizontal-to-vertical spectral ratio (H/V) for detecting the site amplification effects. Moreover, the large variability affecting the H/V spectral ratios for stations located in the epicentral area suggests that these ratios are probably influenced by source-related effects.

In conclusion, source, path and site parameters found in this study are useful to characterize the ground motion observed during the L'Aquila seismic sequence and can

be important elements for future studies spanning from source-related studies to strong-motion modeling to hazard assessments.

Acknowledgments

We used the records made available by Monitoraggio del Territorio e gestione banche dati of the DPC - Ufficio Valutazione, Prevenzione e Mitigazione del Rischio Sismico (SISM). This work has been carried out within the DPC-INGV S4 (2007-2009) project. Dino Bindi conducted this work during a one-year visiting period at GFZ.

References

Ameri, G., Massa, M., Bindi, D., D'Alema, E., Gorini, A., Luzi, L., Marzorati, S., Pacor, F., Paolucci,R., Puglia R. & Smerzini, C., 2009. The 6 April 2009, M_w 6.3, L'Aquila (Central Italy) earthquake: strong-motion observations, submitted to Seism. Res. Letter Atkinson, G.M. & Mereu, R., 1992. The shape of ground motion attenuation curves in southeastern Canada, Bull. Seismol. Soc. Am., 82, 2014–2031.Bindi, D., Castro, R. R., Franceschina, G., Luzi, L., & Pacor, F., 2004. The 1997–1998 Umbria–Marche sequence (Central Italy): source, path and site effects estimated from strong motion data recorded in the epicentral area, J. Geophys. Res. 109, B04312, doi:10.1029/2003JB002857.

Bosi C., & Bertini, T., 1970. Geologia della media valle dell'Aterno, Mem. Soc. Geol. It., IX, 719-777.

Brune, J.N., 1970. Tectonic stress and the spectra of seismic shear waves from earthquakes. J. Geophys. Res. 75, 4997–5009.

Burger, R.W., Somerville, P.G., Barker, J.S.,. Herrmann, R.B & Helmberger, D.V., 1987. The effect of crustal structure on strong ground motion attenuation relations in eastern North America, Bull. Seismol. Soc. Am., 77, 420–439.

Castro, R. R., Anderson, J. G.&. Singh, S.K., 1990. Site response attenuation and source spectra of S waves along the Guerrero, Mexico, subduction zone, Bull. Seism. Soc. Am. 80, 1481–1503.

CEN (2004). Eurocode 8: Design of structures for earthquake resistance - Part 1: General rules, seismic actions and rules for buildings, Comité Européen de Normalisation Brussels, May.

Gruppo di Lavoro MPS, (2004). Redazione della mappa di pericolosità sismica prevista dall'Ordinanza PCM del 20 marzo 2003. Rapporto Conclusivo per il Dipartimento dellaProtezione Civile, INGV, Milano-Roma, aprile 2004, 65 pp. + 5 appendixes.

Hanks, T. C. & Kanamori, H., 1979. A moment magnitude scale, J. Geophys. Res. 84, 2348–2350.

Hanks, T. & McGuire, T., 1981. The character of high-frequency strong ground motion. Bull. Seism. Soc. Am. 71, 2071–2095

Keilis-Borok, V., 1959. On the estimation of the displacement in an earthquake source and of source dimension, Ann. Geofis., 12, 205– 214.

Konno, K. & Ohmachi, T., 1998. Ground-motion characteristic estimated from spectral ratio between horizontal and vertical components of microtremor, Bull. Seism. Soc. Am. 88, 228–241.

Lermo, J. & Chavez-Garcia, F.C., (1993). Site effect evaluation using spectral ratios with only one station. Bull. Seism. Soc. Am. 83, 1574–1594.

Luzi L., Hailemikael S., Bindi D., Pacor, F. & F. Mele (2008). ITACA (ITalian ACcelerometric Archive): a web portal for the dissemination of Italian strong motion data. Seism ResLett. doi:10.1785/gssrl.79.5

Massa, M., Pacor, F., Luzi, L., Bindi, D., Milana, G., Sabetta, F., Gorini, A. & Marcucci,S., 2009. The Italian Accelerometric Archive: data set and data processing, submitted to Bull. Earth. Eng.

Mori, J., & Helmberger, D., 1996. Large-amplitude Moho reflections (SmS) from Landers aftershocks, southern California, Bull. Seism. Soc. Am. 86, 1845–1852.Ponziani,

F., R. De Franco, Minelli, G., Biella, G., Federico, c. & Pialli, G., 1995. Crustal shortening and duplication of the Moho in the Northern Appennines: A view from seismic refraction data, Tectonophysics, 252, 391–418.

Rovelli, A., Bonamassa, O., Cocco, M., Di Bona, M. & Mazza, S., 1988. Scaling laws and spectral parameters of the ground motions in active extensional areas in Italy, Bull. Seismol. Soc. Am., 78, 530–560.

Sommerville, P. & Yoshimura, J., 1990. The influence of critical Moho reflections on strong ground motions recorded in San Francisco and Oakland during the 1989 Loma Prieta earthquake, Geophys. Res. Lett., 17, 1203– 1206.

Figure captions

Figure 1 Map showing the epicenters of considered earthquakes (red stars) and recording stations (grey circles); the mainshock recording at station AQK is also displayed. The focal solution is taken from the Global Centroid Moment Tensor Project (http://www.globalcmt.org)

Figure 2 Top. Non-parametric S-wave spectral attenuation versus distance (gray curves). The results for four selected frequencies are shown as black lines. The decay proportional to the inverse of distance (dashed line) is shown for reference. Bottom. Frequency dependence of the quality factor Q for distances between 6 and 50 km (gray line) and best least-square fit model (black line). The value of the geometrical spreading exponent is n=0.75.

Figure 3 Site amplifications obtained by the generalized inversion technique (GIT) for the north-south (NS) component (black line), the vertical (V) component (dark gray line) and considering the NS-to-V spectral ratio (dashed line). For each station, the Eurocode 8 (EC8) site classification is also reported (CEN, 2004). The star in the site class indicates that $Vs_{,30}$ was indirectly estimated from other geological/geophysical information [http://itaca.mi.ingv.it].

Figure (4) Top. Displacement source spectra (black lines) obtained from inversion and best fit Brune models (grey lines). Bottom. Seismic moment versus source radius (squares), compared with constant-stress drop predictions (black lines).

Table 1. Source parameters of the considered earthquakes.

Id	Event Date yymmdd_hhmmss	$^{+}M_w$	$M_w^{(est)}$	Mo [Nm]	f_c [Hz]	Ro [km]	$\Delta\sigma$ [MPa]	$\Delta\sigma_{RMS}$ [MPa]
1	20090406_013239	6.3	6.3	3.42e+18*	0.24	5.46	9.2	10.7
2	20090406_023704	5.1	4.8	2.10 e+16	1.39	0.94	11.3	13.4
3	20090406_163809	4.4	4.3	3.17e+15	2.15	0.61	6.2	7.8
4	20090406_231537	5.1	4.8	1.90 e+16	1.56	0.84	14.3	16.5
5	20090407_092628	5.0	4.8	1.74 e+16	1.32	0.99	7.8	9.3
6	20090407_174737	5.6	5.5	2.52e+17*	0.70	1.87	16.8	20.0
7	20090407_213429	4.6	4.5	8.25e+15	1.39	0.93	4.4	4.6
8	20090408_225650	4.1	4.1	1.85e+15	2.97	0.44	9.6	9.6
9	20090409_005259	5.4	5.4	1.60e+17*	0.70	1.86	10.9	15.6
10	20090409_031452	4.4	4.4	5.55e+15	2.14	0.61	10.7	10.6
11	20090409_043244	4.2	4.4	4.70e+15	1.38	0.94	2.4	2.5
12	20090409_193816	5.3	5.2	7.50e+16*	0.87	1.49	9.8	17.3
13	20090413_211424	5.1	4.8	1.84e+16	1.36	0.96	9.2	10.3

$^{+}$ is the values in this column are taken from RCMT-INGV (http://www.bo.ingv.it/RCMT/). The seismic moments denoted with star are constrained to the values provided by Harvard-CMT (http:// www.globalcmt.org).

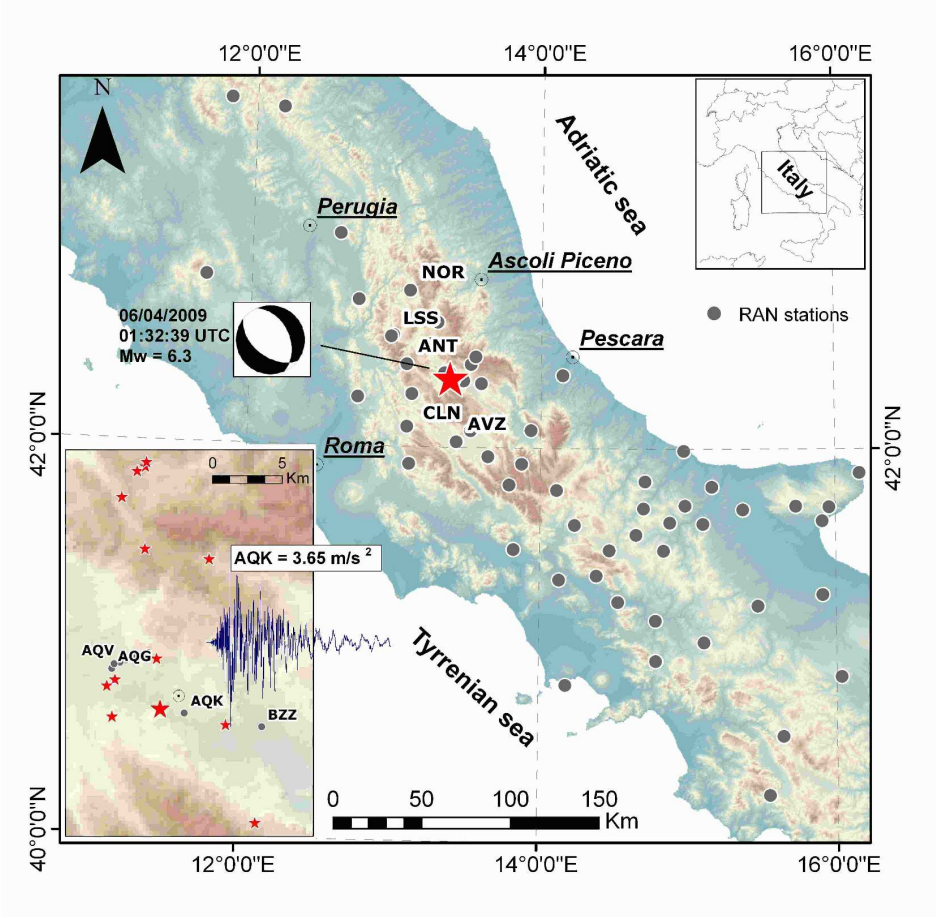

Figure 1

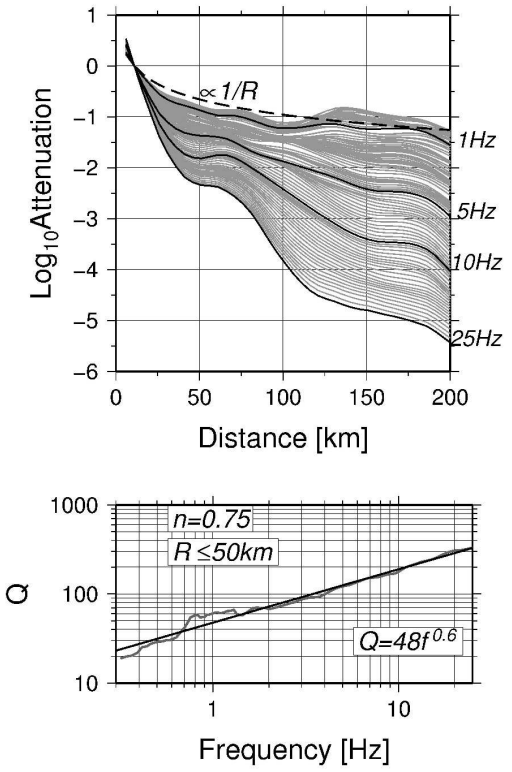

Figure 2

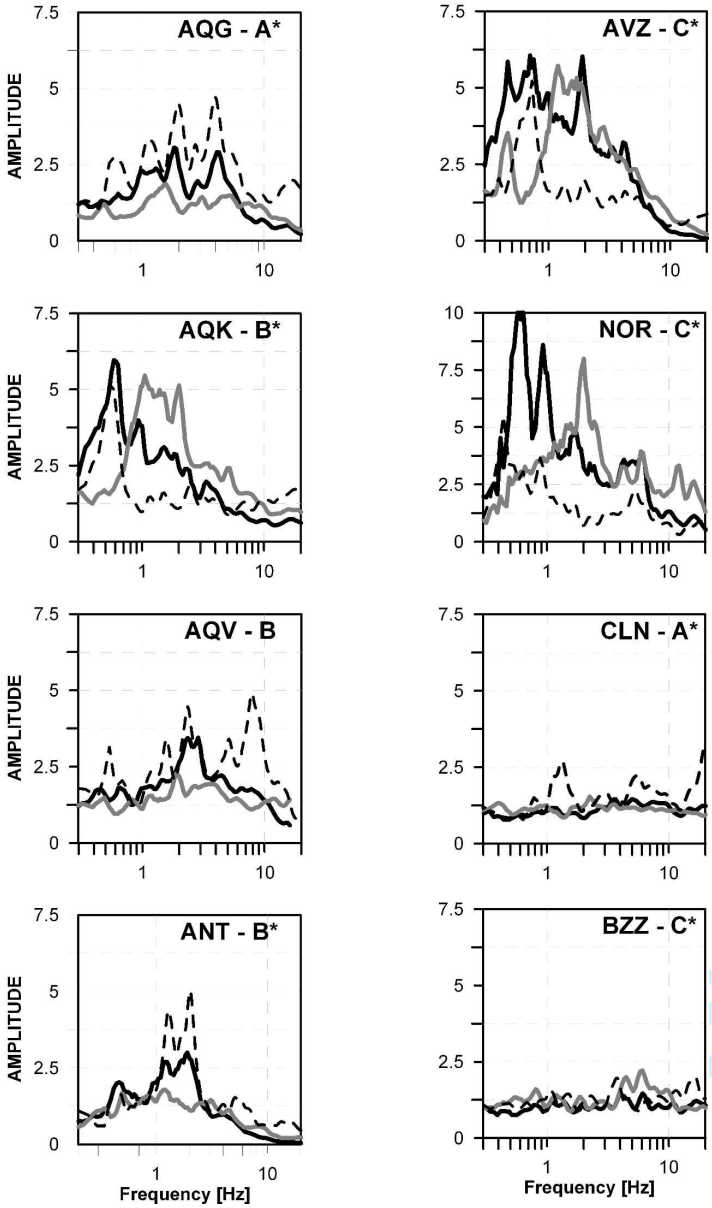
AQG - A*
AVZ - C*
AQK - B*
NOR - C*
AQV - B
CLN - A*
ANT - B*
BZZ - C*
AMPLITUDE
Frequency [Hz]

Figure 3

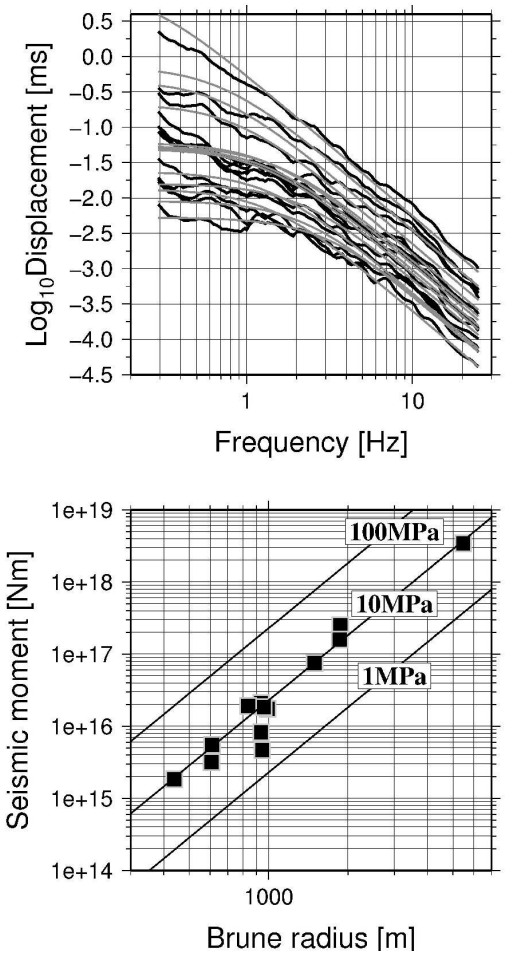

Figure 4

Supplementary materials

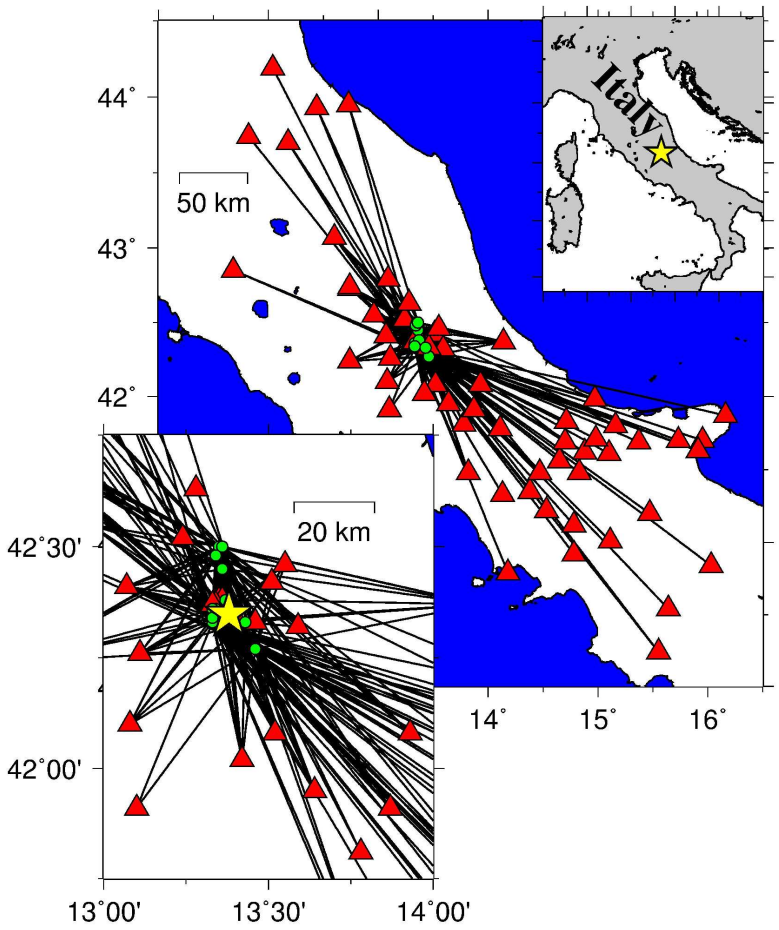

Figure SM1. Path coverage for the stations (triangles) and earthquakes (circles) analyzed in the manuscript. The star indicates the epicentre of the mainshock.

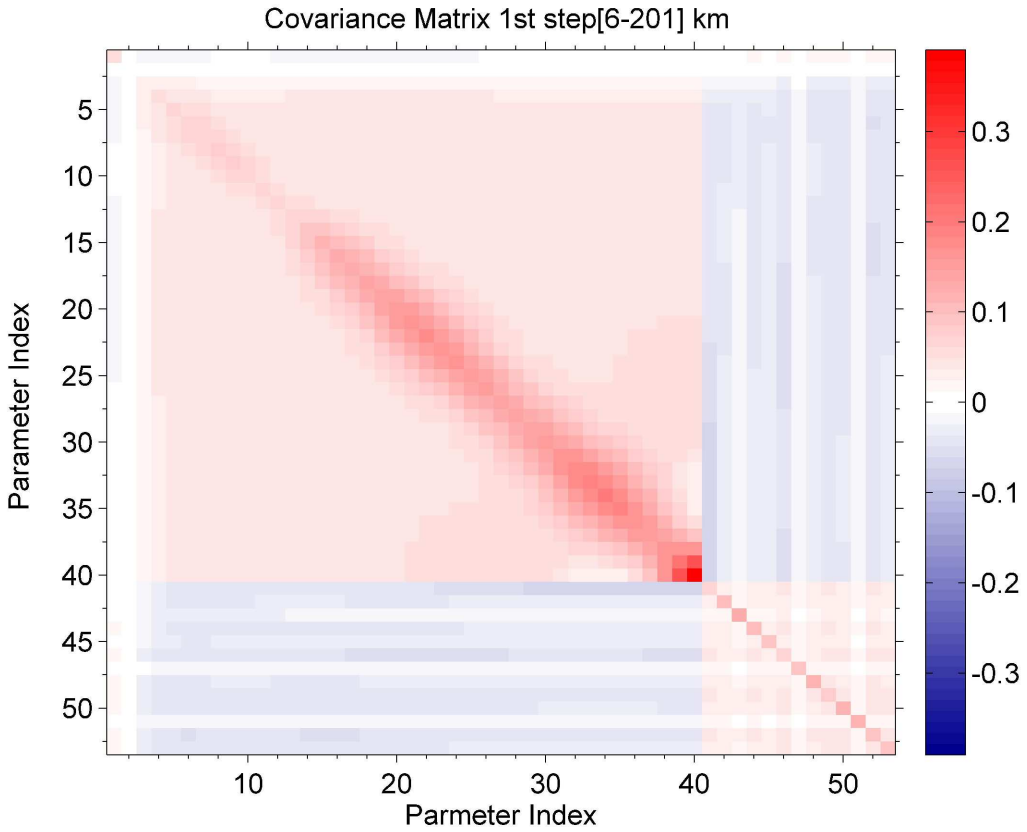

Figure SM2 Unit covariance matrix computed for the first step of the GIT inversion (see equation 1), considering hypocentral distances up to 200 km and setting the spatial resolution to 5 km. The parameter indexes from 1 to 40 are relevant to attenuation bins whereas those from 41 to 53 to earthquakes.

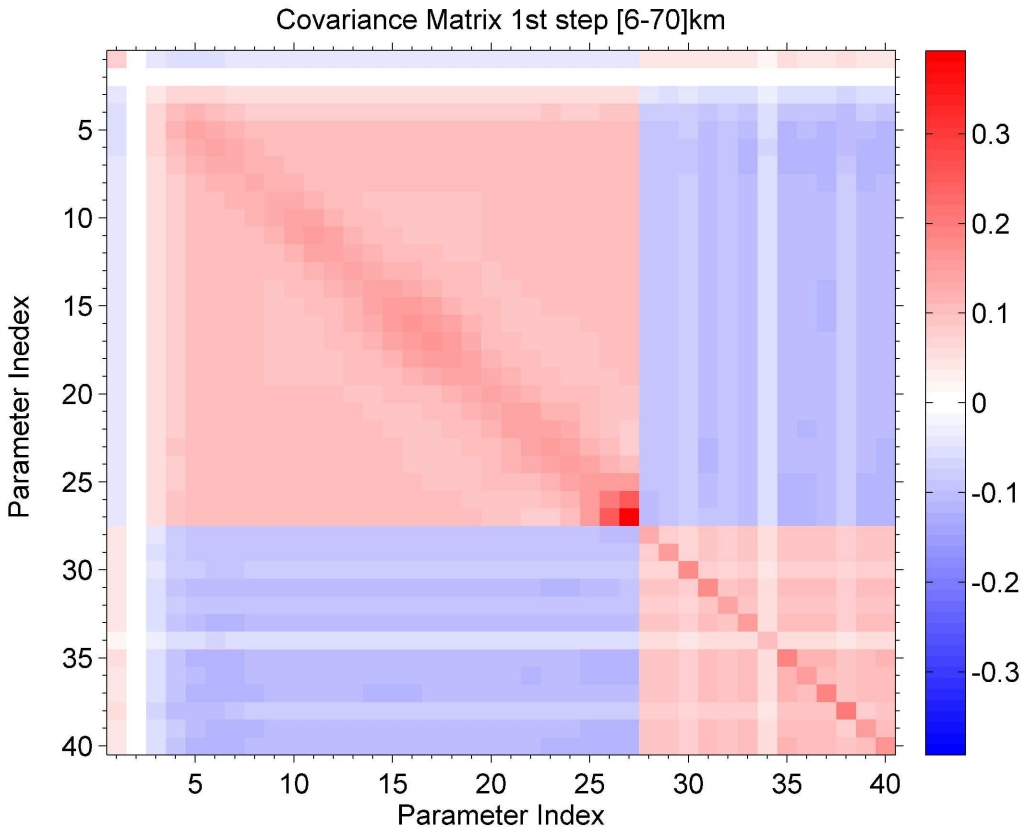

Figure SM3 Unit covariance matrix computed for the first step of the GIT inversion (see equation 1), considering hypocentral distances up to 70 km and setting the spatial resolution to 2.5 km. The parameter indexes from 1 to 29 are relevant to attenuation bins whereas those from 27 to 40 to earthquakes.

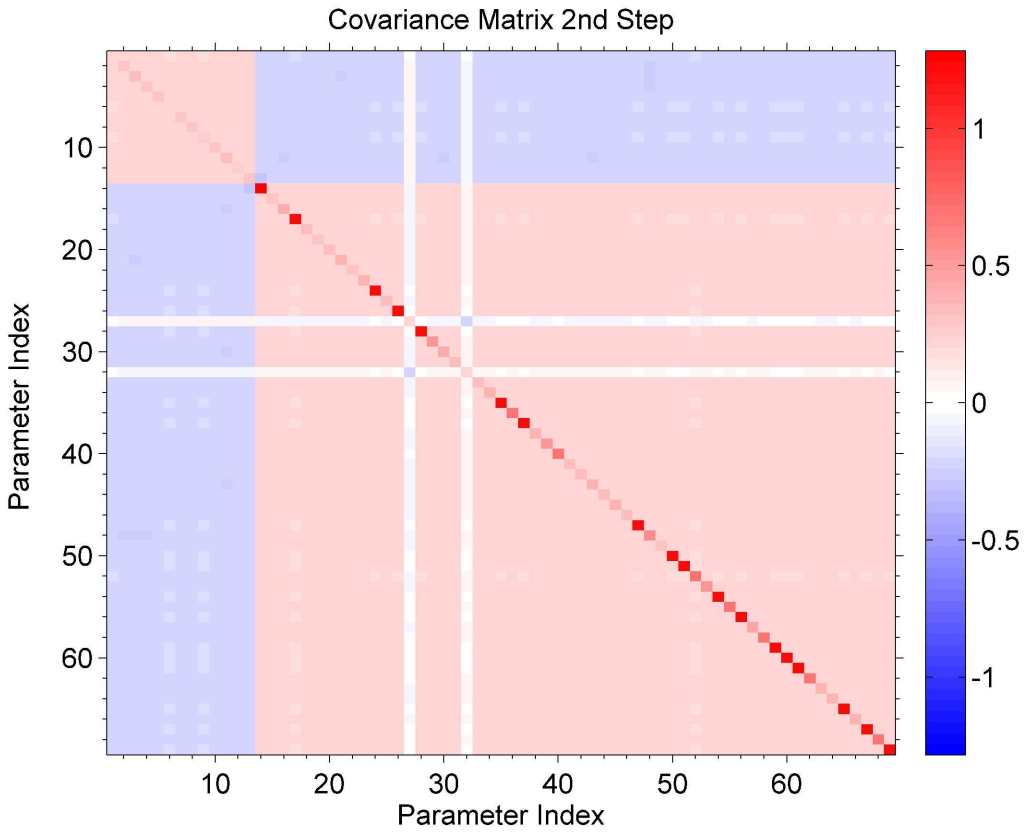

Figure SM4 Unit covariance matrix computed for the second step of the GIT inversion (see equation 2). The parameter indexes from 1 to 13 are relevant to earthquakes whereas those from 14 to 69 to stations.

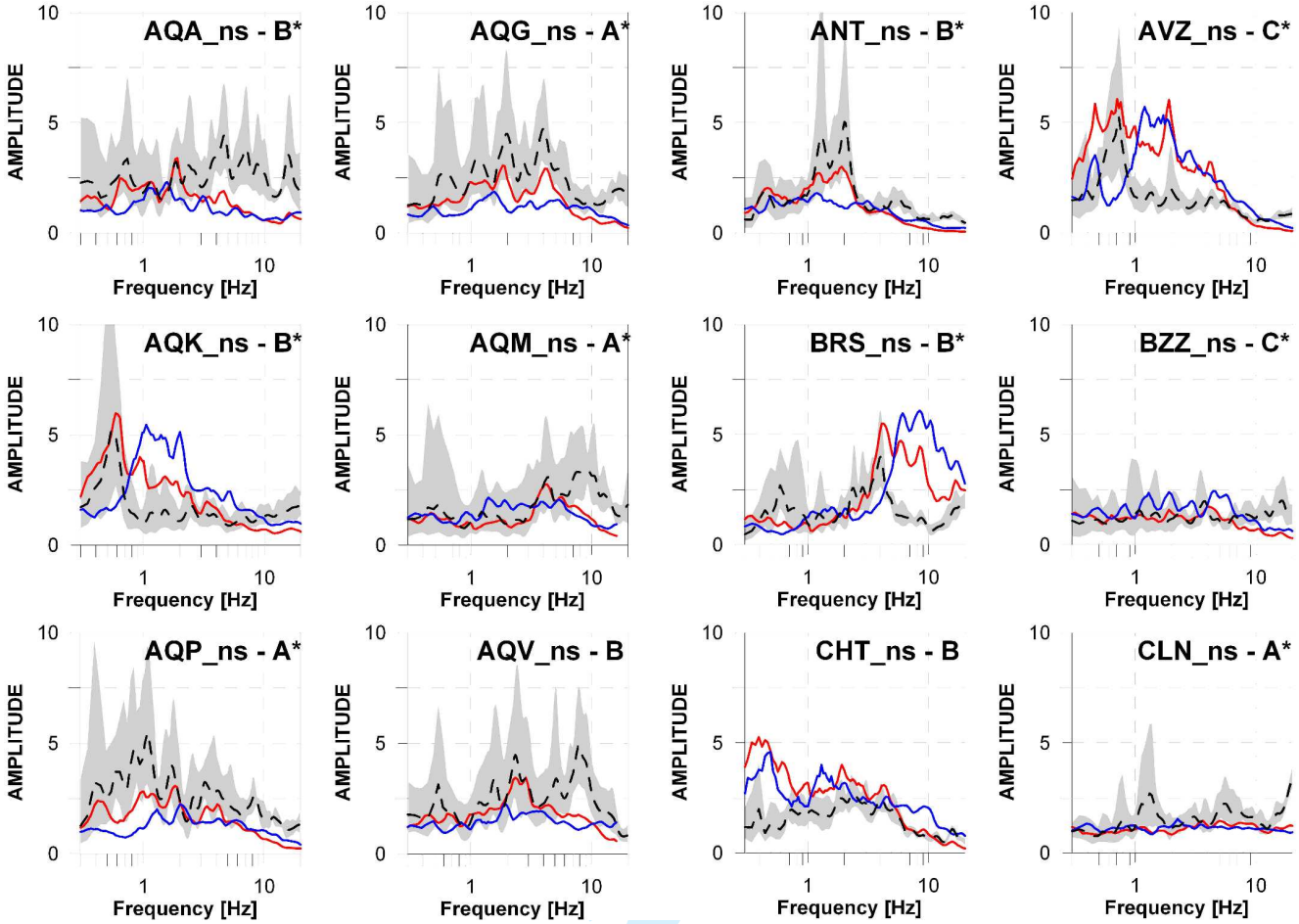

Figure SM5 Site amplification effects estimated for 12 different stations. The station name and the relevant site classification, selected accordingly to the EC8 provision code, in given in the upper right corner of each panel. The average (black dashed line) ± one standard deviation (gray area) of the north-south to vertical spectral ratios are compared with the GIT results for the north-south (red) and vertical (blue) components.

.

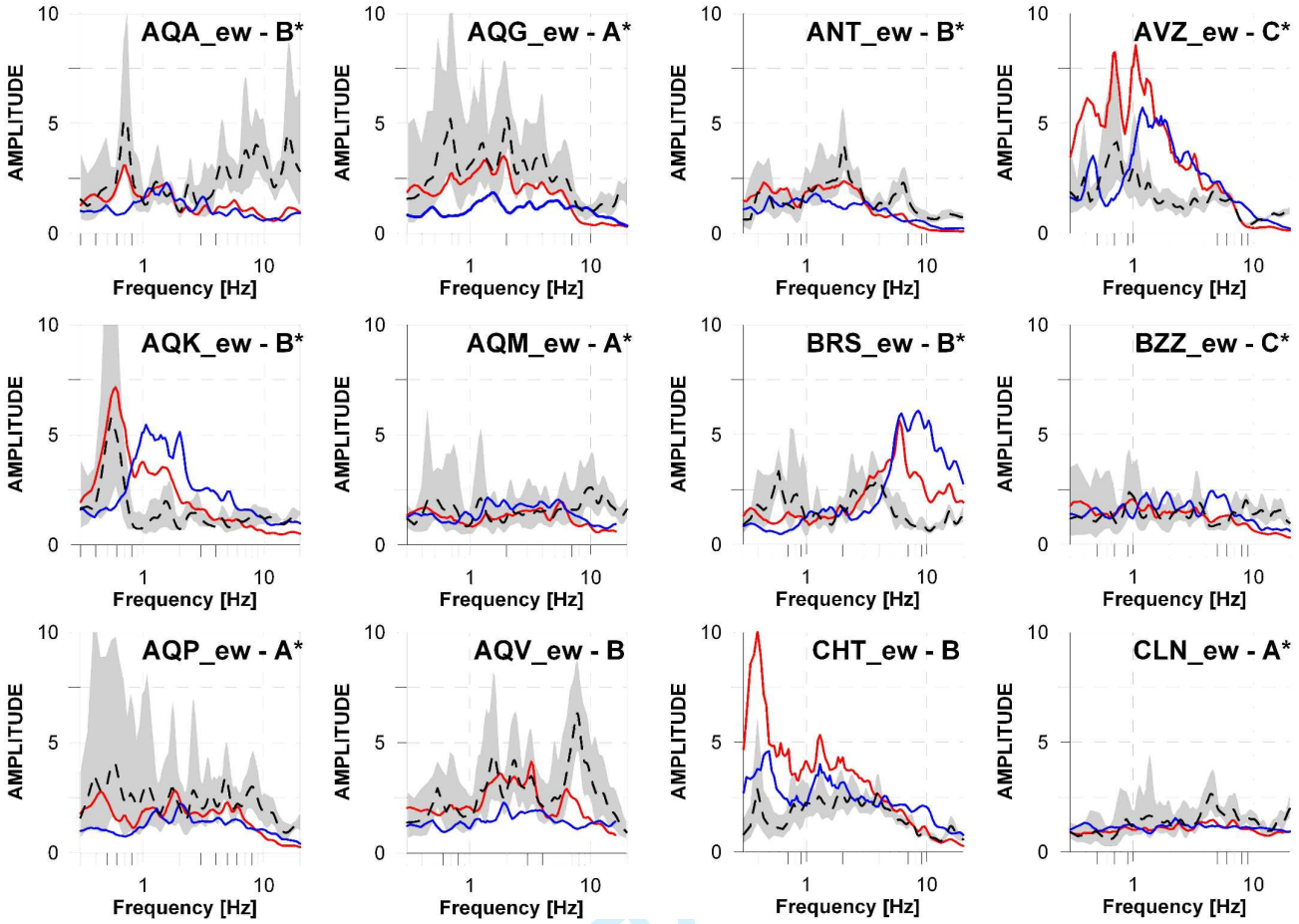

Figure SM6 The same as in Figure SM5 but considering the east-west component

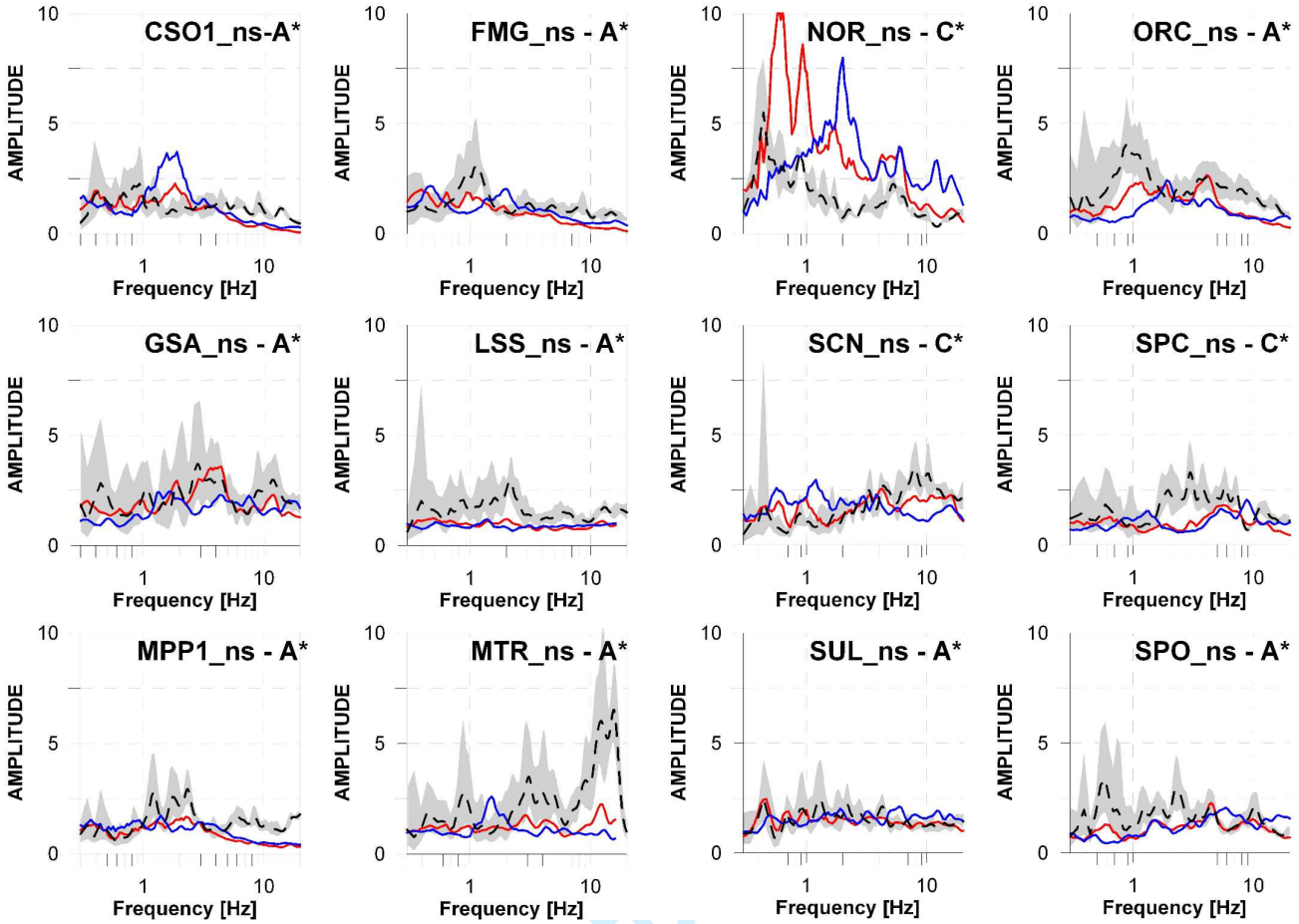

Figure SM7 The same as in Figure SM5 but considering 12 different stations

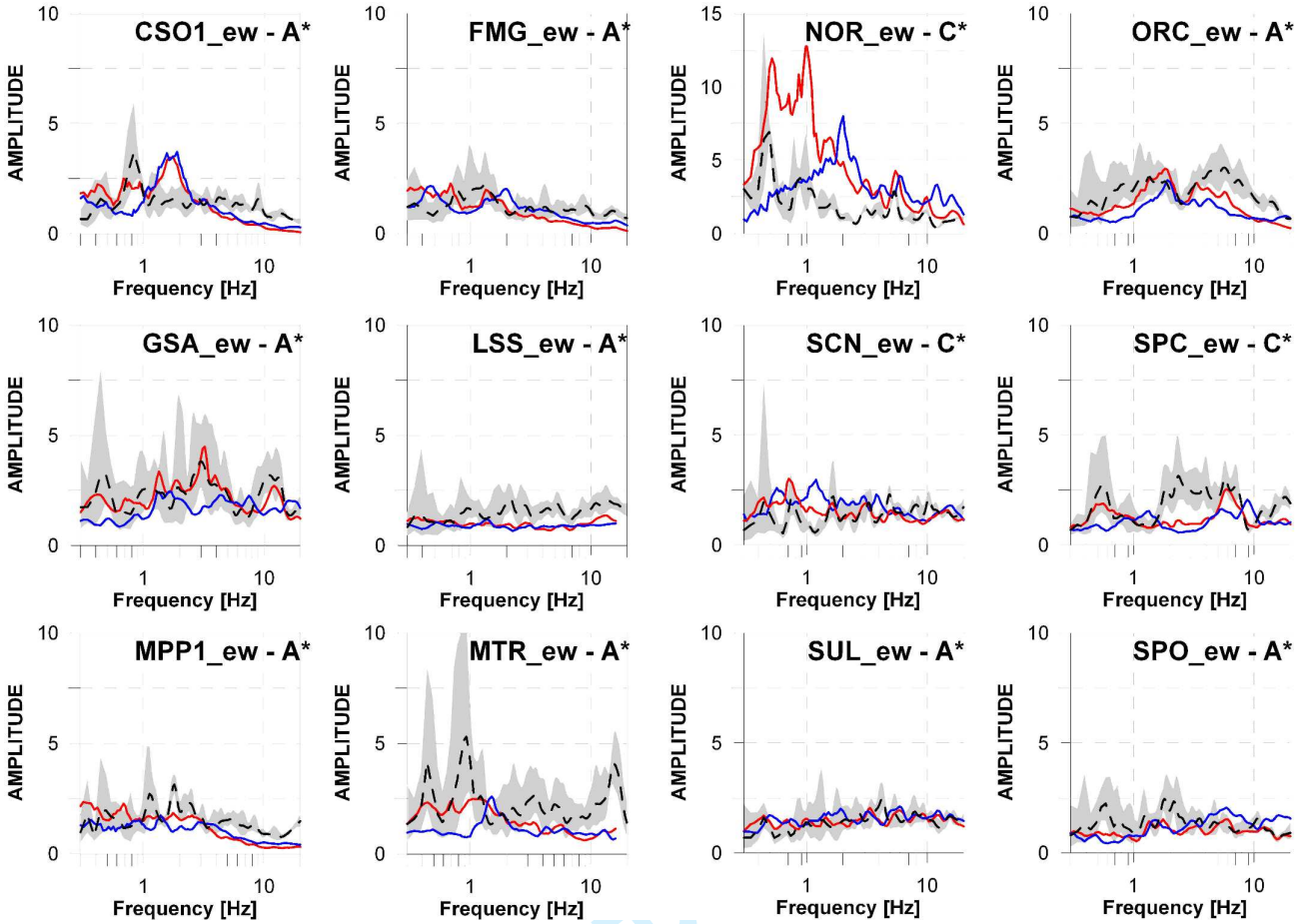

Figure SM8 The same as in Figure SM6 but considering 12 different stations